Research Article

URF PUBLISHERS
connect with research world

Journal of Petroleum & Chemical Engineering

https://urfpublishers.com/journal/petrochemical-engineering

Vol: 3 & Iss: 2

Dynamic Studies of Glioblastoma Multiforme

Lakshmi N Sridhar*

Chemical Engineering Department, University of Puerto Rico, Mayaguez, PR 00681-9046, USA

Citation: Sridhar LN. Dynamic Studies of Glioblastoma Multiforme. *J Petro Chem Eng* 2025;3(2):72-78.

Received: 01 April, 2025; **Accepted:** 05 May, 2025; **Published:** 07 May, 2025

***Corresponding author:** Lakshmi N Sridhar, Chemical Engineering Department, University of Puerto Rico, Mayaguez, PR 00681-9046, USA

ABSTRACT

Glioblastoma multiforme (GBM) is a devastating brain cancer which is fatal. The treatment the dynamics of GBM is very complex and the mathematical models involving GBM are very nonlinear. Multiobjective nonlinear model predictive control in conjunction with bifurcation analysis on the truncated and full models without and with various protein complexes The MATLAB program MATCONT was used to perform the bifurcation analysis. The MNLMPC calculations were performed using the optimization language PYOMO in conjunction with the state-of-the-art global optimization solvers IPOPT and BARON. The bifurcation analysis revealed limit points the limit were beneficial because they allowed the multiobjective nonlinear model predictive control calculations to converge to the Utopia point which is the best possible solution. Additionally, for the MNLMPC calculations, it is shown that both the truncated and full models give identical answers.

Keywords: Bifurcation; Optimization; Control; Cancer tumour; Glioblastoma

Introduction

Glioblastoma multiforme (GBM) is a deadly type of type of brain cancer that results in death within 1.5 years of diagnosis. There has been a lot of theoretical work that deal with optimal strategies to control this devastating disease. Many models have been developed describing the dynamic interactions between the cancer cells and the various treatments used to destroy the cancerous cells. The dynamics of this interaction is highly complex and nonlinear. Bifurcation analysis has been used by several workers to understand this complexity. Additionally, rigorous optimal control procedures have been used to maximize the elimination of the cancer cells while minimizing the costs involved. The aim of this work is to perform multiobjective nonlinear model predictive control in conjunction with bifurcation analysis on full and truncated models with and without the various protein complexes that are involved.

Background

Xu and co-workers[1] developed a novel strategy to overcome drug resistance associated with mitochondrial respiratory defect and hypoxia. Kaufman, et al.[2] demonstrated the Glioma expansion in collagen matrices: analyzing collagen concentration-dependent growth and motility patterns. Farin, et al.[3] developed a dynamic analysis showing that transplanted glioma cells migrate and proliferate on host brain vasculature: a dynamic analysis.

Furnari, et al.[4] discussed genetics, biology and paths to treatment for malignant astrocytic glioma. Stein and co-workers[5] developed a mathematical model of glioblastoma tumor spheroid invasion in a three-dimensional in vitro experiment. Beadle and co-workers[6] discussed the role of myosin II in glioma invasion of the brain. Godlewski, et al[7] showed that targeting of the BMI-1 oncogene/stem cell renewal factor by microRNA-128 inhibits glioma proliferation and self-renewal.

Kim, et al.[8] demonstrated that epidermal growth factor-induced enhancement of glioblastoma cell migration in 3D arises from an intrinsic increase in speed but an extrinsic matrix and proteolysis-dependent increase in persistence.

Sen, et al.[9] discussed isoform-specific contributions of a-cctinin to glioma cell mechanobiology. Kim and co-workers[10] developed a mathematical model of Brain tumor: pattern formation of glioma cells outside the tumor spheroid core. Godlewski and co-workers[11] developed a conditional switch controlling glioma cell proliferation and migration. Godlewski, et al.[12] showed that mircroRNA-451 regulates LKB1/AMPK signaling and allows glioma cells to adapt to metabolic stress. Kim, et al.[13] developed a mathematical model describing miR451 and AMPK Mutual Antagonism in Glioma Cell Migration and Proliferation.

Wesseling, et al.[14] discuss the pathological diagnosis of diffuse gliomas: towards a smart synthesis of microscopic and molecular information in a multidisciplinary context. Kim[15] described the regulation of cells considering proliferation and migration in Glioblastoma using a therapeutic strategy. Kim and Roh[16] developed a hybrid model describing cell proliferation and migration in glioblastoma. Dhruv, et al.[17] showed that the reciprocal activation of transcription factors underlies the dichotomy between the proliferation and invasion of glioma cells. Pyonteck, et al.[18] concluded that the inhibition alters macrophage polarization and blocks glioma progression. Xie, et al.[19] provided an overview of proliferation and invasion targeting adaptive glioblastoma. Lamszus, et al.[20] discussed links between cellular function, glucose metabolism and the glioma microenvironment. Kim, et al.[21] developed strategies for eradicating Glioma Cells using a Multi-Scale Mathematical Model with miR-451-AMPK-mTOR control.

De los Reyes, et al.[22] developed optimal control strategies of eradicating invisible glioblastoma cells after conventional surgery. Han, et al.[23] investigated TGF-beta signaling and its targeting for glioma treatment. Goodwin and co-workers[24] researched Extra neural Glioblastoma Multiforme Vertebral Metastasis. Duzgun, et al.[25] discussed the role of mTOR in glioblastoma while Lee, et al.[26] studied the role of myosin II in glioma invasion. Rajesh and co-workers[27] studied glioma progression through the prism of heat shock protein mediated extracellular matrix epithelial to mesenchymal transition. Kim, et al.[28] investigated the role of extracellular matrix and microenvironment in regulation of tumor growth and LAR-mediated invasion in glioblastoma. Esmaeili, et al.[29] the Direction of Tumor Growth in Glioblastoma Patients. Krol, et al.[30] was able to detect circulating tumor cell clusters in human glioblastoma. Jung, et al.[31] developed strategies in regulating glioblastoma signaling pathways and anti-invasion therapy.

In this work, the model described in Jung, et al.[31] is used and multiobjective nonlinear model predictive control in conjunction with bifurcation analysis on full and truncated models with and without the various protein complexes. The model equations are first described. Then the numerical strategies for bifurcation analysis and multiobjective nonlinear model predictive control procedures are presented followed by the results and discussion and conclusions.

Model Equations

The model equations Jung, et al.[31] are

$$\frac{dGval}{dt} = u_1(t) - \mu_G Gval$$

$$\frac{dMval}{dt} = Gval - Mval + \frac{l_1 l_2^2}{l_2^2 + \alpha Aval^2} \quad (1)$$

$$\varepsilon_1 \frac{dAval}{dt} = S_1 - Aval + \frac{l_3 k_4^2}{l_4^2 + \beta Mval^2}$$

$$\varepsilon_2 \frac{dRval}{dt} = S_2 - Rval + \frac{l_5 k_6^2}{l_6^2 + \gamma e^{-Dval} Aval^2}$$

$$\frac{dDval}{dt} = u_2(t) - \mu_D Dval$$

$$\frac{d[CycB]}{dt} = k1 - \left(k_2^{'} + \left(k_2^{''}[Cdh1]\right)\right) + ((p27/p21)HIF)[CcyB]\Big)$$

$$\frac{d[Cdh1]}{dt} = \frac{\left(k_3^{'} + \left(k_3^{*}[P55Cdca]\right)\right)(1-[Cdh1])}{(j_3 + 1 - [Cdh1])} - \frac{\left((k_4[mass_s][Cycb][Cdh1])\right)}{(j_4 + [Cdh1])}$$

$$\frac{d[P55Cdct]}{dt} = k_5^{'} + \frac{(k_5^{''}(([Cycb][mass_s)^n))}{((j5^n) + (([Cycb][mass_s)^n))} - (k_6[P55Cdct])$$

$$\frac{d[P55Cdca]}{dt} = \frac{\left(k_7[plk1]([P55Cdct] - [P55Cdca])\right)}{(j_7 + [P55Cdct] - [P55Cdca])} - \frac{(k_8[MAD][P55Cdca}{(j8 + cdca)}$$

$$\frac{d[Plk1]}{dt} = k_9[mass_s][Cycb](1 - [Plk1])) - (k_{10}[Plk1])$$

$$\frac{d[mass]}{dt} = \mu^{+}[mass](1 - \frac{[mass]}{m^{*}})$$

Gval represents the glucose that regulates Mval, the miR-451 (M). Aval represents AMPK and Rval is the mTOR with the signaling pathway to cell cycle dynamics. Dval represents the drug that suppresses the inhibition of mTOR by AMPK. CyCB and Cdh1 represent the Cyclin B complex and the APC-Cadherin 1 complex.

The active form of the p55cdc-Anaphase-promoting complex is represented by $[p55cdcA]$ and the total p55cdc-Anaphase-promoting complex is $[p55cdcT]$. The active form of Polo-like kinase 1 protein is $[Plk1]$ and the cell mass is represented by $[mass]$. $[mass_s]$ is the pseudo mass given by

$$[mass_s] = [mass] + \frac{\varsigma_1 (\frac{1}{R})^{n1}}{(K_m)^{n1} + (\frac{1}{R})^{n1}} \quad (2)$$

The parameter values are

$\mu_G = 0.5; \mu_D = 1.316; l_1 = 4; l_2 = 1; l_3 = 4; l_4 = 1; l_5 = 4; l_6 = 1; \alpha = 1.6; \beta = 1; S_1 = 0.2;\ S_2 = 1.2;$
$\varepsilon_1 = 0.02; \varepsilon_2 = 0.02; \gamma = 1;\ k_1 = 0.12;\ k_2^{'} = 0.12;\ k_2^{*} = 4.5;\ p27/p21 = 1.05;$
$k = 0.01; k_3^{'} = 3;\ k_3^{''} = 30;\ k_4 = 105;\ j_3 = 0.04;\ j_4 = 0.04;\ k_5^{'} = 0.015;\ k_5^{*} = 0.6;\ k_6 = 0.3;\ j_5 = 0.3;$
$n = 4;\ k_7 = 3; k_8 = 1.5;\ j_7 = 0.001;\ j_8 = 0.001;\ [MAD] = 1;\ k_9 = 0.3;\ k_{10} = 0.06; mu^{+} = 0.03;$
$m^{*} = 10;\ \varepsilon = 0.006; \varsigma_1 = 2.5;\ n_1 = 10;\ K_m = 0.5;\ \varsigma_2 = 1;\ n_2 = 10;\ K_H = 10;\ [HIF] = 0.9091;$

These parameters represent glucose consumption rate, drug decay rate, miR-451 autocatalytic production rate, Hill-type coefficient AMPK autocatalytic production rate, Hill-type coefficient, AMPK autocatalytic production rate, Hill-type coefficient, inhibition strength of miR-451 by AMPK complex, inhibition strength of AMPK complex by miR-451, signalling source of AMPK, signalling source of mTOR, scaling factor (slow dynamics) of AMPK complex, scaling factor (slow dynamics) of mTOR, inhibition strength of AMPK complex by miR-451 , production rate of [CycB] , the degradation rate of [CycB], the degradation rate of [CycB] by [Cdh1] inhibitory effect of p21 or p27 genes, oxygen concentration threshold, activation rate of [Cdh1], the activation rate of [Cdh1] by [p55cdcA], inactivation rate of [Cdh1] by [CycB], Michaelis-

Menten activation constant, Michaelis-Menten inactivation constant, production rate of [p55cdcT] transcription rate of [p55cdcT] by [CycB], the degradation rate of [p55cdcT], the dissociation constant of [p55cdcT], Hill coefficient, activation rate of [p55cdcA], inactivation rate of [p55cdcA], Michaelis-Menten activation constant, Michaelis-Menten inactivation constant, spindle checkpoint genes concentration, the activation rate of [Plk1] by [CycB], the degradation rate of [Plk1], specific growth rate, maximum size to which a cell may grow, cell cycle heterogeneity growth rate parameter, Hill-type parameter, Hill-type parameter, Hill-type parameter, Hill-type parameter, Hill-type parameter and the Hypoxia-inducible factor.

u_1, u_2 are both bifurcation parameters and control values.

Bifurcation Analysis

The existence of multiple steady-states and limit cycles in various processes has led to much research involving bifurcation analysis. Multiple steady states occur because of the existence of branch and limit points. Hopf bifurcation points cause limit cycles. One of the most commonly used software to locate limit points, branch points and Hopf bifurcation points is the MATLAB program MATCONT[32,33]. This software detects Limit points (LP), branch points (BP) and Hopf bifurcation points(H). Consider an ODE system

$$\frac{dx}{dt} = f(x,\alpha) \quad (3)$$

$x \in R^n$ Let the tangent plane at any point x be $W = [w_1, w_2, w_3, w_4, ...w_{n+1}]$. The bifurcation parameter is α. Define matrix A as

$$A = [\partial f / \partial x \quad | \partial f / \partial \alpha] \quad (4)$$

where $\partial f / \partial x$ is the Jacobian matrix. Since the gradient is orthogonal to the tangent vector,

$$Aw = 0 \quad (5)$$

For both limit and branch point the matrix $[\partial f / \partial x]$ must be singular. For a limit point (LP) the n+1 th component of the tangent vector $w_{n+1} = 0$ and for a branch point (BP) the matrix $\begin{bmatrix} A \\ w^T \end{bmatrix}$ must be singular. At a Hopf bifurcation point,

$$\det(2 f_x(x,\alpha) @ I_n) = 0 \quad (6)$$

@ indicates the bialternate product while I_n is the n-square identity matrix. Hopf bifurcations cause limit cycles and should be eliminated because limit cycles make optimization and control tasks very difficult. More details can be found in Kuznetsov[34,35] and Govaerts[36].

Multiobjective Nonlinear Model Predictive Control

The multiobjective nonlinear model predictive control (MNLMPC) method[37] used in these calculations is rigorous and does not involve weighting functions or additional constraints. Let $\sum_{t_{i=0}}^{t_i=t_f} q_j(t_i)$ (j=12..n) be the variables that need to be minimized/maximized simultaneously for a problem involving a set of ODE

$$\frac{dx}{dt} = F(x,u)$$

t_f being the final time value and n the total number of objective variables. u is the control parameter. The MNLMPC method first solves the single objective optimal control problem independently optimizing each of the variables $\sum_{t_{i=0}}^{t_i=t_f} q_j(t_i)$ individually. The minimization/maximization of $\sum_{t_{i=0}}^{t_i=t_f} q_j(t_i)$ will lead to the values q_j^*. Then the optimization problem that will be solved is

$$\min\left(\sum_{j=1}^{n}\left(\sum_{t_{i=0}}^{t_i=t_f} q_j(t_i) - q_j^*\right)\right)^2$$

$$subject\ to \quad \frac{dx}{dt} = F(x,u);$$

This will provide the values of u at various times. The first obtained control value of u is implemented and the rest are discarded. This procedure is repeated until the implemented and the first obtained control values are the same or if the Utopia point where ($\sum_{t_{i=0}}^{t_i=t_f} q_j(t_i) = q_j^*$ for all j) is obtained. The optimization package in Python, Pyomo[38], where the differential equations are automatically converted to a Nonlinear Program (NLP) using the orthogonal collocation method will be used. The resulting nonlinear optimization problem was solved using the solvers IPOPT[39] and confirmed as a global solution with BARON[40]. To summarize the steps of the algorithm are as follows

Optimize $\sum_{t_{i=0}}^{t_i=t_f} q_j(t_i)$ subject to the differential and algebraic equations that govern the process using Pyomo with IPOPT and BARON. This will lead to the value q_j^* at various time intervals t_i. The subscript *i* is the index for each time step.

Minimize $\left(\sum_{j=1}^{n}\left(\sum_{t_{i=0}}^{t_i=t_f} q_j(t_i) - q_j^*\right)\right)^2$ subject to the differential and algebraic equations that govern the process using Pyomo with IPOPT and BARON. This will provide the control values for various times.

Implement the first obtained control values and discard the remaining.

Repeat steps 1 to 3 until there is an insignificant difference between the implemented and the first obtained value of the control variables or if the Utopia point is achieved. The Utopia point is when $\sum_{t_{i=0}}^{t_i=t_f} q_j(t_i) = q_j^*$ or for all j. This implies that

$(\sum_{j=1}^{n}(\sum_{t_i=0}^{t_i=t_f} q_j(t_i)-q_j^*))^2=0$. Sridhar[41] proved that the MNLMPC calculations to converge to the Utopia solution when the bifurcation analysis revealed the presence of limit and branch points. This was done by imposing the singularity condition on the co-state equation[42].

This is illustrated with a simple two-variable example. Let $\sum_{t_i=0}^{t_i=t_f} q_1(t_i)=\hat{q}_1$ and $\sum_{t_i=0}^{t_i=t_f} q_2(t_i)=\hat{q}_2$ If the minimization of $\hat{q}_1$ lead to the value q_1^* and the minimization of $\hat{q}_2$ lead to the value q_2^* The MNLPMC calculations will minimize the function $(\hat{q}_1-q_1^*)^2+(\hat{q}_2-q_2^*)^2$. The multiobjective optimal control problem is

$$\min \quad (\hat{q}_1-q_1^*)^2+(\hat{q}_2-q_2^*)^2 \quad \textit{subject to} \quad \frac{dx}{dt}=f(x,u)$$

Simple differentiation shows that

$$\frac{d}{dx_i}((\hat{q}_1-q_1^*)^2+(\hat{q}_2-q_2^*)^2)=2(\hat{q}_1-q_1^*)\frac{d}{dx_i}(\hat{q}_1-q_1^*)+2(\hat{q}_2-q_2^*)\frac{d}{dx_i}(\hat{q}_2-q_2^*)$$

The Utopia point requires that both $(\hat{q}_1-q_1^*)$ and $(\hat{q}_2-q_2^*)$ are zero. Hence

$$\frac{d}{dx_i}((\hat{q}_1-q_1^*)^2+(\hat{q}_2-q_2^*)^2)=0$$

The optimal control co-state equation[36] is

$$\frac{d}{dt}(\lambda_i)=-\frac{d}{dx_i}((\hat{q}_1-q_1^*)^2+(\hat{q}_2-q_2^*)^2)-f_x\lambda_i; \quad \lambda_i(t_f)=0$$

λ_i is the Lagrangian multiplier. t_f is the final time. The first term in this equation is 0 and hence

$$\frac{d}{dt}(\lambda_i)=-f_x\lambda_i;\lambda_i(t_f)=0$$

At a limit or a branch point, for the set of ODE $\frac{dx}{dt}=f(x,u)$ f_x is singular. Hence there are two different vectors-values for $[\lambda_i]$ where $\frac{d}{dt}(\lambda_i)>0$ and $\frac{d}{dt}(\lambda_i)<0$. In between there is a vector $[\lambda_i]$ where $\frac{d}{dt}(\lambda_i)=0$. This coupled with the boundary condition $\lambda_i(t_f)=0$ will lead to $[\lambda_i]=0$ This makes the problem an unconstrained optimization problem and the only solution is the Utopia solution.

Results and Discussion

The original model has eleven ordinary differential equations (Eq. 1). Since the first 5 equations of this model were self-sufficient (the other variables are not present in the first five equations) the truncated model was first considered. The effects of the chemical protein comlexes were not considered. The model equations for the truncated model are

$$\frac{dGval}{dt}=u_1(t)-\mu_G Gval$$
$$\frac{dMval}{dt}=Gval-Mval+\frac{l_1 l_2^2}{l_2^2+\alpha Aval^2}$$
$$\varepsilon_1\frac{dAval}{dt}=S_1-Aval+\frac{l_3 k_4^2}{l_4^2+\beta Mval^2}$$
$$\varepsilon_2\frac{dRval}{dt}=S_2-Rval+\frac{l_5 k_6^2}{l_6^2+\gamma e^{-Dval}Aval^2}$$
$$\frac{dDval}{dt}=u_2(t)-\mu_D Dval$$

u_1, u_2 are used as the bifurcation parameters individually. For the truncated model (Eq. 14) two limit points were found for each of the bifurcation parameters u_1, u_2.

When u_1 was used as the bifurcation parameter the two limit points for the co-ordinates of $(Gval, Mval, Aval, Rval, Dval, u_1)$ were label = LP, x = (0.575313, 1.285868, 1.707468, 2.227386, 0.007599, 0.287656) and (0.391657, 2.517522, 0.745114, 3.778995, 0.007599, 0.195828). This is shown in **(Figure 1)**.

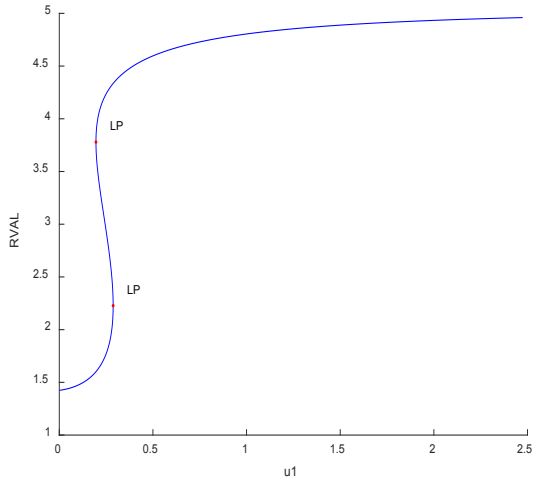

Figure 1: Bifurcation (truncated model u1 vs Rval).

When u_2 was used as the bifurcation parameter the two limit points for the co-ordinates of $(Gval, Mval, Aval, Rval, Dval, u_2)$ were label = LP, x = (0.100000, 0.770732, 2.709366, 2.175070, 0.861295, 1.133465) and (0.100000, 2.457341, 0.768301, 3.986453, 0.304074, 0.400161). This is shown in **(Figure 2)**.

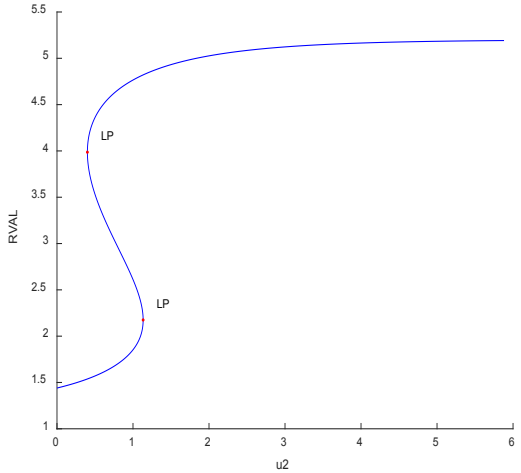

Figure 2: bifurcation truncated model (u2 vs Rval).

When the full model (Eq. 1) was considered for bifurcation analysis one limit point was found for each of the bifurcation

parameters u_1, u_2 in the feasible region (where none of the variables were negative) . When u_1 was used as the bifurcation parameter, for the full model, the limit point for the co-ordinates of $(Gval, Mval, Aval, Rval, Dval, [CycB], [Cdh1], [P55Cdct], [P55Cdca], [Plk1], [mass], u_1)$ were (0.290144, 0.493394, 3.416887, 2.303891, 1.492932, 0.078886, 0.099250, 0.050546, 0.000464, 0.161636, 0.000000, 0.145072) **(Figure 3)**.

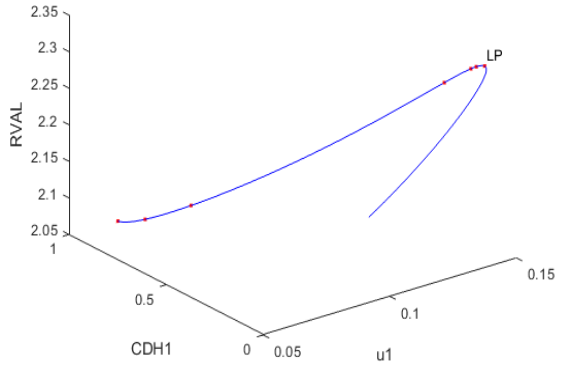

Figure 3: Bifurcation (full model u1 CDH1 Rval).

When u_2 was used as the bifurcation parameter for the full model, the limit point for the co-ordinates of $(Gval, Mval, Aval, Rval, Dval, [CycB], [Cdh1], [P55Cdct], [P55Cdca], [Plk1], [mass], u_2)$ were (0.100000, 0.253415, 3.958625, 2.303891, 1.787266, 0.078886, 0.099250, 0.050546, 0.000464, 0.161636, 0.000000, 2.352042) **(Figure 4)**.

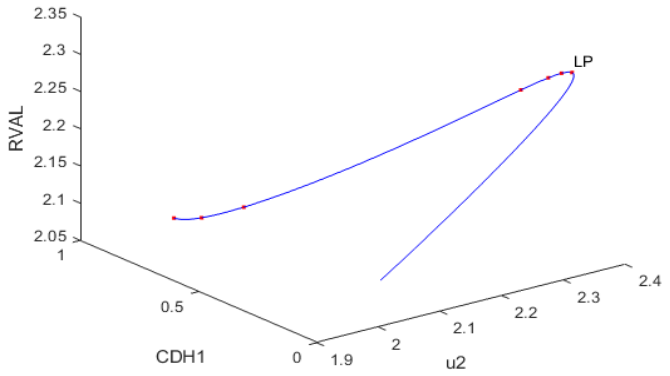

Figure 4: Bifurcation (full model u2 CDH1 Rval).

For the MNLMPC $\sum_{t_i=0}^{t_i=t_f}(MVAL)(t_i)$ and $\sum_{t_i=0}^{t_i=t_f}(RVAL)(t_i)$ were individually maximized, resulting in a value of 10 for the full and truncated problems. The Multiobjective problem involved the minimization of $(\sum_{t_i=0}^{t_i=t_f}(MVAL)(t_i)-10)^2+(\sum_{t_i=0}^{t_i=t_f}(RVAL)(t_i)-10)^2$ and resulted in the utopia value of 0 for both the truncated and full problems (confirming the analysis of Sridhar, 2024). u_1, u_2 are used as the control values together. The first obtained values of u_1, u_2 were implemented and the rest were discarded. This procedure was repeated until there was an insignificant difference between the implemented and the first obtained value of the control variables. The obtained MNLMPC control values of u_1, u_2 were 0.08966 and 0.943536 in both the truncated and full problems.

For the MNLMPC calculations, both the truncated and full models gave identical answers for the Gval Mval Aval Rval Dval and u_1, u_2 This was because the Lagrangian multiplier was 0 in both cases since both the truncated and full models exhibit limit points, confirming the analysis of Srihdar[41]. All the MNLMPC profiles are shown in **(Figures 5-10)**.

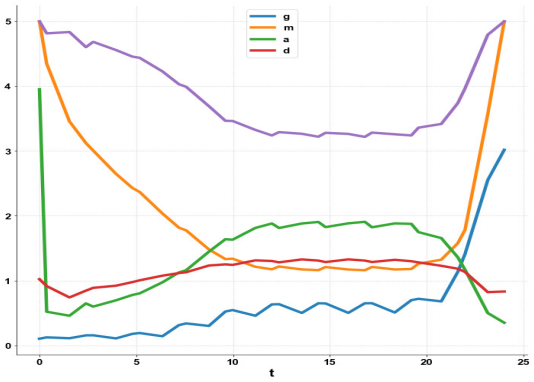

Figure 5: MNLMPC (Gval, Mval, Aval, Rval, Dval).

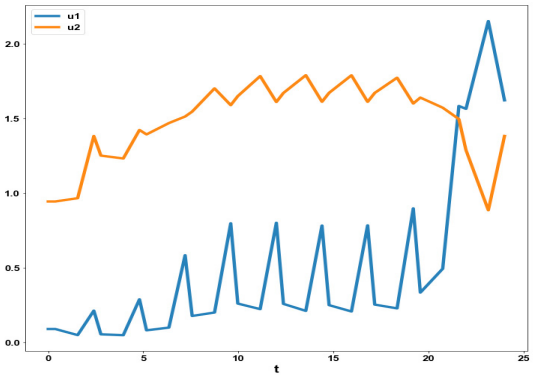

Figure 6: MNLMPC (U1 U2).

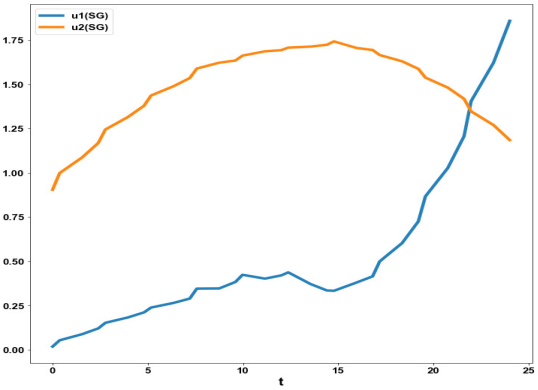

Figure 7: MNLMPC (u1 u2 with savitzky Golay filter).

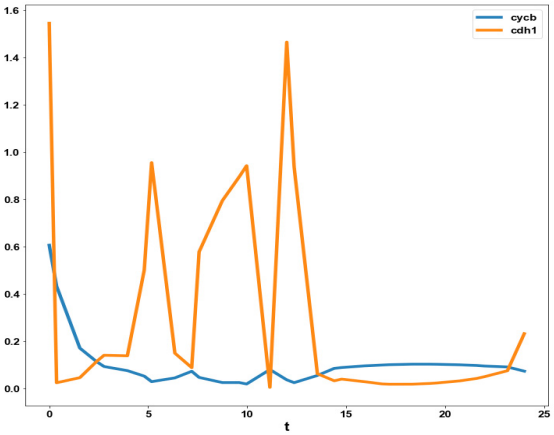

Figure 8: MNLMPC (CYCB and CDH1).

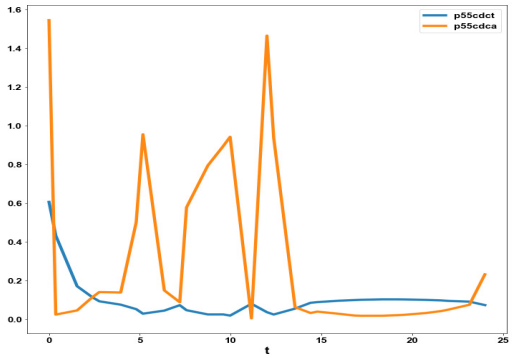

Figure 9: MNLMPC(p55cdct and p55cdca).

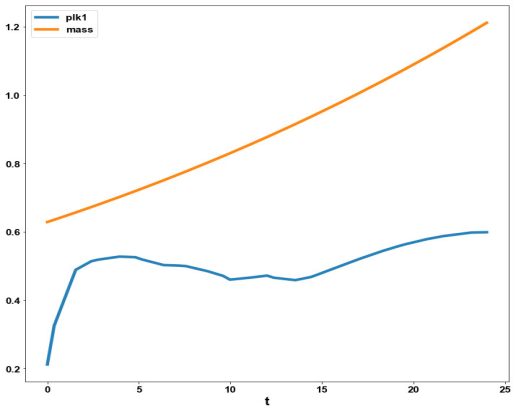

Figure 10: MNLMPC (PLk1 and mass).

Conclusions

Multiobjective nonlinear model predictive control in conjunction with bifurcation analysis on the truncated and full models without and with various protein complexes. The bifurcation analysis reveals the existence of limit points. These limit points cause the Lagrangian multipliers in the multiobjective nonlinear model predictive control calculations to go to 0 yielding the utopia solution. Additionally, for the MNLMPC calculations, both the truncated and full models gave identical answers confirming that the Lagrangian multipliers were 0 for both the models.

Data Availability Statement

All data used is presented in the paper.

Conflict of Interest

The author, Dr. Lakshmi N Sridhar has no conflict of interest.

Acknowledgement

Dr. Sridhar thanks Dr. Carlos Ramirez and Dr. David Suleiman for their encouragement.

References

1. Xu RH, Pelicano H, Zhou Y, et al. Inhibition of glycolysis in cancer cells: a novel strategy to overcome drug resistance associated with mitochondrial respiratory defect and hypoxia. Cancer Res 2005;65(2):613-621.
2. Kaufman LJ, Brangwynne CP, Kasza KE, et al. Glioma expansion in collagen I matrices: analyzing collagen concentration-dependent growth and motility patterns. Biophys J BioFAST 2005;89:635-650.
3. Farin A, Suzuki SO, Weiker M, et al. Transplanted glioma cells migrate and proliferate on host brain vasculature: a dynamic analysis. Glia 2006;53(8):799-808.
4. Furnari FB, Fenton T, Bachoo RM, et al. Malignant astrocytic glioma: genetics, biology and paths to treatment. Genes Dev 2007;21(21):2683-2710.
5. Stein AM, Demuth T, Mobley D, Berens M, Sander LM. A mathematical model of glioblastoma tumor spheroid invasion in a three-dimensional in vitro experiment. Biophys J 2007;92(1):356-365.
6. Beadle C, Assanah MC, Monzo P, Vallee R, Rosenfield SS, Canoll P. The role of myosin II in glioma invasion of the brain. Mol Biol Cell 2008;19:3357-3368.
7. Godlewski J, Nowicki MO, Bronisz A, et al. Targeting of the BMI-1 oncogene/stem cell renewal factor by microRNA-128 inhibits glioma proliferation and self-renewal. Cancer Res 2008;68(22):9125-1930.
8. Kim HD, Guo TW, Wu AP, Wells A, Gertler FB, Lauffenburger DA. Epidermal growth factor-induced enhancement of glioblastoma cell migration in 3D arises from an intrinsic increase in speed but an extrinsic matrix and proteolysis-dependent increase in persistence. Mol Biol Cell 2008;19:4249-4259.
9. Sen S, Dong M, Kumar S. Isoform-specific contributions of a-cctinin to glioma cell mechanobiology. PLoS One 2009;4(12):8427.
10. Kim Y, Lawler S, Nowicki MO, Chiocca EA, Friedman A. A mathematical model of Brain tumor: pattern formation of glioma cells outside the tumor spheroid core. J Theor Biol 2009;260:359-371.
11. Godlewski J, Bronisz A, Nowicki MO, Chiocca EA, Lawler S. microRNA-451: A conditional switch controlling glioma cell proliferation and migration. Cell Cycle 2010; 9(14):2742-2748.
12. Godlewski J, Nowicki MO, Bronisz A, et al. MircroRNA-451 regulates LKB1/AMPK signaling and allows adaptation to metabolic stress in glioma cells. Molecular Cell 2010;37:620-632.
13. Kim Y, Roh S, Lawler S, Friedman A. miR451 and AMPK Mutual Antagonism in Glioma Cell Migration and Proliferation: A Mathematical Model. PLoS One 2011;6(12):1-10.
14. Wesseling P, Kros JM, Jeuken JWM. The pathological diagnosis of diffuse gliomas: towards a smart synthesis of microscopic and molecular information in a multidisciplinary context. Diagnostic Histopathology 2011;17(11):486-494.
15. Kim Y. Regulation of Cell Proliferation and Migration in Glioblastoma: New Therapeutic Approach. Frontiers in Oncology 2013;3:53.
16. Kim Y, Roh S. A hybrid model for cell proliferation and migration in glioblastoma. Discrete & Continuous Dynamical Systems-B 2013;18:969-1015.
17. Dhruv HD, Winslow WSM, Armstrong B, et al. Reciprocal activation of transcription factors underlies the dichotomy between proliferation and invasion of glioma cells. PLoS One 2013;8(8):72134.
18. Pyonteck SM, Akkari L, Schuhmacher AJ, et al. CSF-1R inhibition alters macrophage polarization and blocks glioma progression. Nat Med 2013;19(10):1264-1272.
19. Xie Q, Mittal S, Berens ME. Targeting adaptive glioblastoma: an overview of proliferation and invasion. Neuro Oncol. 2014; 16(12):1575-1584.
20. Lamszus K, MD, Kathagen A, Holz M, Schulte A, Westphal M. Go Or Grow-Links Between Cellular Function, Glucose Metabolism and Glioma Microenvironment. NeuroOncol 2014;16(3):36.
21. Kim Y, Powathil G, Kang H, et al. Strategies of Eradicating Glioma Cells: A Multi-Scale Mathematical Model with MiR-451-AMPK-mTOR Control. PLoS One 2015;10(1):1-30.

22. de los Reyes VAA, Jung E, Kim Y. Optimal control strategies of eradicating invisible glioblastoma cells after conventional surgery. J Royal Society Interface 2015;12(106).

23. Han J, Alvarez-Breckenridge CA, Wang QE, Yu J. TGF-beta signaling and its targeting for glioma treatment. Am J Cancer Res 2015;5(3):945-55.

24. Goodwin CR, Liang L, Abu-Bonsrah N, et al. Extra neural Glioblastoma Multiforme Vertebral Metastasis. World Neurosurg 2016; 89:578-582.

25. Duzgun Z, Eroglu Z, Avci CB. Role of mTOR in glioblastoma. Gene 2016;575(2):187-190.

26. Lee W, Lim S, Kim Y. The role of myosin II in glioma invasion: A mathematical model. PLoS One 2017;12(2):0171312.

27. Rajesh Y, Biswas A, Mandal M. Glioma progression through the prism of heat shock protein mediated extracellular matrix remodeling and epithelial to mesenchymal transition. Exp Cell Res 2017;359(2):299-311.

28. Kim Y, Kang H, Powathil G, et al. Role of extracellular matrix and microenvironment in regulation of tumor growth and LAR-mediated invasion in glioblastoma. PLoS One 2018;13(10):1-40.

29. Esmaeili M, Stensjoen AL, Berntsen EM, Solheim O, Reinertsen I. The Direction of Tumor Growth in Glioblastoma Patients. Sci Rep 2018; 8(1):1199.

30. Krol I, Castro-Giner F, Maurer M, et al. Detection of circulating tumor cell clusters in human glioblastoma. Br J Cancer 2018;119(4):487-491.

31. Jung E, de los Reyes VAA, Pumares KJA, Kim Y. Strategies in regulating glioblastoma signaling pathways and anti-invasion therapy. PLoS ONE 2019;14(4):0215547.

32. Dhooge A, Govearts W, Kuznetsov AY. MATCONT: A Matlab package for numerical bifurcation analysis of ODEs. ACM transactions on Mathematical software 2003;29(2):141-164.

33. Dhooge A, Govaerts W, Kuznetsov YA, Mestrom W, Riet AM. CL_MATCONT; A continuation toolbox in Matlab 2004.

34. Kuznetsov YA. Elements of applied bifurcation theory. Springer 1998.

35. Kuznetsov YA. Five lectures on numerical bifurcation analysis. Utrecht University 2009.

36. Govaerts WJF. Numerical Methods for Bifurcations of Dynamical Equilibria 2000.

37. Flores-Tlacuahuac A. Pilar Morales and Martin Riveral Toledo; Multiobjective Nonlinear model predictive control of a class of chemical reactors. I & EC research 2012:5891-5899.

38. William EH, Laird CD, Watson JP, Woodruff DL, Hackebeil GA, Nicholson BL, Siirola JD. Pyomo - Optimization Modeling in Python. Second Edition 2017;67.

39. Wächter A, Biegler L. On the implementation of an interior-point filter line-search algorithm for large-scale nonlinear programming. Math Program 2006;106:25-57.

40. Tawarmalani M, Sahinidis NV. A polyhedral branch-and-cut approach to global optimization, Mathematical Programming 2005;103(2):225-249.

41. Sridhar LN. Coupling Bifurcation Analysis and Multiobjective Nonlinear Model Predictive Control. Austin Chem Eng 2024;10(3):1107.

42. Ranjan US. Optimal control for chemical engineers. Taylor and Francis 201.